23rd ABCM International Congress of Mechanical Engineering
December 6-11, 2015, Rio de Janeiro, RJ, Brazil

ANALYSIS OF THE DYNAMIC BEHAVIOR OF A ROTOR SYSTEM UNDER BASE EXCITATION

Marcelo Samora Sousa Jr
Aldemir Ap Cavalini Jr
Valder Steffen Jr

LMEst - Laboratory of Mechanics and Structures, Federal University of Uberlândia, School of Mechanical Engineering, Av. João Naves de Ávila, 2121, Uberlândia, MG, 38408-196, Brazil.
marcelosamora@mec.ufu.br

Abstract. *In this paper, a preliminary investigation regarding the dynamic behavior of a rotor system subjected to a base excitation is presented numerically. The rotating machine is composed by a horizontal flexible shaft, one rigid disc, and two self-aligning ball bearings. A mathematical model of the rotor is derived from the Lagrange's equation and the Rayleigh-Ritz method, which is obtained by considering the strain and kinetic energies of the disc and shaft, and the mass unbalance. The equations of motion of the system are used to provide information about the vibration responses of the rotor under base and unbalance excitations simultaneously. Some simplifications are adopted in order to obtain the responses of the considered rotor system. Therefore, the proposed analysis is performed both in the time and frequency domains, as generated by the orbits, unbalance response, and Campbell diagram. Further research efforts will be dedicated to additional numerical tests considering a finite element model. In addition, experimental studies are under consideration.*

Keywords: *rotor system, simplified rotor model, vibration responses, and Campbell diagram.*

1. INTRODUCTION

According to Ishida and Yamamoto (2012), research on rotordynamics has over 140 years of history. Its beginning was marked with the work of WJ Macquorn Hankine (Hankine, 1869), in which the author mistakenly stated that it is impossible for rotating machines operating above a certain speed. This speed was later called critical speed for Dunkerley (1984). Simplified basics about rotating machines were approached by Jeffcott (1919). The work of HH Jeffcott led to the development of other essential researches, such as the Campbell diagram firstly presented by Wilfred Campbell from General Electric. More effective methods of balancing were proposed and the behavior of rotors supported by hydrodynamic bearings was further investigated, leading to the design of lighter rotating machines operating at higher speeds.

The mathematical representation of the specific physical phenomena that involve rotating machines requires a reliable design tool. In this context, the finite element (FE) method appears as a largely used technique for rotordynamics design. Nelson and MacVaugh (1976) were among the first researchers to include the effects of rotational inertia, gyroscopic moment, and axial force in the FE models. Before the FE method, the so-called transfer matrix method was used to determine the dynamic behavior of rotating machines considering the system as continuous one (Lallement, Lecoanet, Steffen Jr, 1982). In this context, the modern rotating systems currently employed in various industrial sectors were developed, such as steam turbines, hydro power units, and aircraft engines.

Regarding the aeronautical applications, the aircraft engine is considered a typical onboard rotor which has its dynamic behavior influenced by external excitations (i.e., base excitations). A mathematical model able to faithfully represent the dynamic behavior of onboard rotors is obtained considering various subsystems, as follows: firstly, the subsystems that can be defined by its geometry, such as the shaft (typically modeled from the FE method), discs and couplings; later, the subsystems that are dependent on the frequency and/or lateral displacements and velocities of the shaft, such as rolling or hydrodynamic bearings, the gyroscopic effect, and clearly the efforts applied in the system through its base. It is worth mentioning that is currently small the number of scientific contributions related to the analysis of rotating machines excited by its base (Dakel, Baguet, Dufour, 2014). Generally, the works on onboard rotors are restricted to rigid shafts (El-Saeidy, Sticher, 2010). Therefore, this paper aims to analyze the dynamic behavior of a flexible rotating machine considering base excitations.

The rotating machine used in this paper is composed by a horizontal flexible shaft, one rigid disc, and two self-aligning ball bearings. The mathematical model of the rotor is derived from the Lagrange's equations and the Rayleigh-Ritz method. According to Lalanne and Ferraris (1998), the main phenomena that occur in rotordynamics can be evaluated by using this kind of model. Regarding the Lagrange's equations, kinetic energy expressions are used to characterize the disc, shaft, and mass unbalance. The flexible shaft is described in terms of strain energy. The forces due to the bearings are incorporated on the Lagrange's equations from its associated virtual work.

2. ROTOR MODELING

Figure 1 shows the schematic representation of the onboard rotor in which three reference frames are used (Duchemin, Berlioz, Ferraris, 2006). $R_0(x_0, y_0, z_0)$ is the inertial frame, $R_s(x_s, y_s, z_s)$ is the frame fixed to the rotor base, and $R(x, y, z)$ is the frame fixed to the disc.

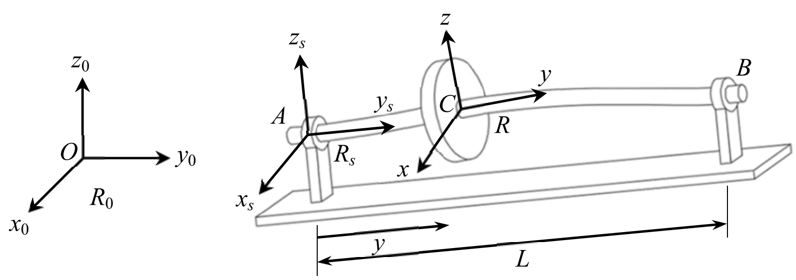

Figure 1. Schematic representation of an onboard rotor (Duchemin, 2003).

The movement of the frame R with respect to R_s is described by the angles ψ, θ, and φ. The orientation of R is defined from a rotation ψ around z_s, a subsequent rotation θ around the new direction x_1, and last by an amount φ around y, as presented by Fig. 2a. Thus, the angular velocity of the frame R with respect to R_s is given by Eq. (1).

$$\vec{\Omega}_R^{R_s} = \begin{Bmatrix} 0 \\ 0 \\ \dot{\psi} \end{Bmatrix}_{R_s} + \begin{Bmatrix} \dot{\theta} \\ 0 \\ 0 \end{Bmatrix}_{R_2} + \begin{Bmatrix} 0 \\ \dot{\phi} \\ 0 \end{Bmatrix}_{R} = \begin{Bmatrix} \dot{\theta}\cos\phi - \dot{\psi}\cos\theta\sin\phi \\ \dot{\phi} + \dot{\psi}\sin\theta \\ \dot{\theta}\sin\phi + \dot{\psi}\cos\theta\cos\phi \end{Bmatrix} \tag{1}$$

where R_2 is an intermediate frame resulting from the imposed angular rotations (Lalanne and Ferraris, 1998).

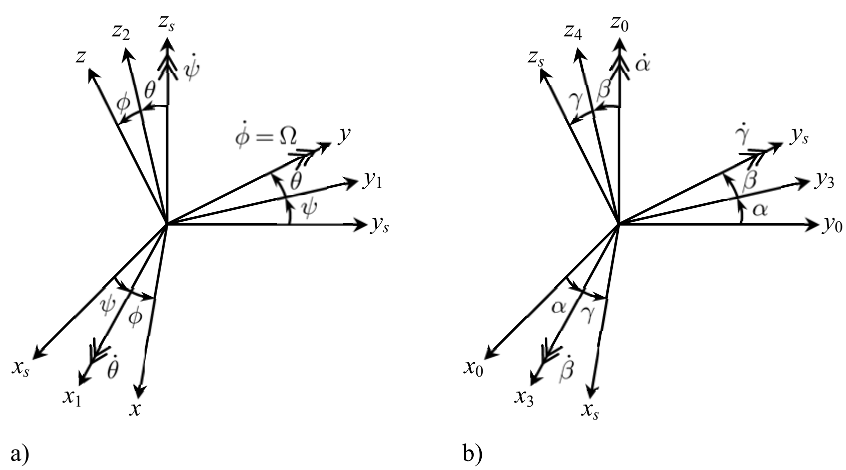

Figure 2. Reference frames for the disc and for the rotor base.

The movement of the base (i.e., frame R_s) with respect to R_0 is defined by the coordinates x_A, y_A, and z_A, and the angles α, β, and γ. The orientation of R_s is defined from a rotation α around z_0, a subsequent rotation β around the new direction x_3, and last by an amount γ around y, as presented by Fig. 2b. Thus, the vector which define the location of the point A (see Fig. 1) and angular velocity of the frame R_s with respect to R_0 are given by Eq. (2) and Eq. (3), respectively.

$$\overrightarrow{OA} = \begin{Bmatrix} x_A \\ y_A \\ z_A \end{Bmatrix}_{R_0} = \begin{Bmatrix} (x_A \cos\alpha + y_A \sin\alpha)\cos\gamma - [z_A \cos\beta + (x_A \sin\alpha - y_A \cos\alpha)\sin\beta]\sin\gamma \\ z_A \sin\beta - (x_A \sin\alpha - y_A \cos\alpha)\cos\beta \\ (x_A \cos\alpha + y_A \sin\alpha)\sin\gamma + [z_A \cos\beta + (x_A \sin\alpha - y_A \cos\alpha)\sin\beta]\cos\gamma \end{Bmatrix}_{R_s} = \begin{Bmatrix} X \\ Y \\ Z \end{Bmatrix}_{R_s} \tag{2}$$

$$\vec{\Omega}_{R_s}^{R_0} = \begin{Bmatrix} 0 \\ 0 \\ \dot{\alpha} \end{Bmatrix}_R + \begin{Bmatrix} \dot{\beta} \\ 0 \\ 0 \end{Bmatrix}_{R_3} + \begin{Bmatrix} 0 \\ \dot{\gamma} \\ 0 \end{Bmatrix}_{R_s} = \begin{Bmatrix} \dot{\beta}\cos\gamma - \dot{\alpha}\cos\beta\sin\gamma \\ \dot{\gamma} + \dot{\alpha}\sin\beta \\ \dot{\beta}\sin\gamma + \dot{\alpha}\cos\beta\cos\gamma \end{Bmatrix}_{R_s} = \begin{Bmatrix} \dot{\alpha}_s \\ \dot{\beta}_s \\ \dot{\gamma}_s \end{Bmatrix}_{R_s} \tag{3}$$

The lateral vibration of the shaft (i.e., movement of frame R fixed to the disk with respect to frame R_s) is described by the translations u and w along x_s and z_s directions, respectively. Additionally, the angles θ and ψ lead to the angular orientation of the shaft with respect to the same directions x_s and z_s, respectively (Duchemin, Berlioz, Ferraris, 2006). Thus, the kinetic energy T_D of the disc (see Fig. 1) can be derived from Eq. (4).

$$T_D = \frac{1}{2} M_D \left(\vec{V}_{CR_s}^{R_0}\right)^2 + \frac{1}{2}\vec{\Omega}_R^{R_0} I_D \vec{\Omega}_R^{R_0} \tag{4}$$

where M_D is the mass of the disc, $\vec{V}_{CR_s}^{R_0}$ is the translational velocity of the disc with respect to R_0 expressed in R_s, $\vec{\Omega}_R^{R_0}$ is the angular velocity vector of the frame R with respect with R_0, and I_D is the tensor of mass inertia moments.

$$\vec{V}_{CR_s}^{R_0} = \left(\frac{d\overrightarrow{OC}}{dt}\right)_{R_s} + \vec{\Omega}_{R_s}^{R_0} \times \left(\overrightarrow{OC}\right)_{R_s} = \begin{Bmatrix} \dot{X} + \dot{u} + \dot{\beta}_s(Z + w) - \dot{\gamma}_s(Y + y) \\ \dot{Y} + \dot{\gamma}_s(X + u) - \dot{\alpha}_s(Z + w) \\ \dot{Z} + \dot{w} + \dot{\alpha}_s(Y + y) - \dot{\beta}_s(X + u) \end{Bmatrix}_{R_s} = \begin{Bmatrix} \dot{u}_C \\ \dot{v}_C \\ \dot{w}_C \end{Bmatrix}_{R_s} \tag{5}$$

$$\vec{\Omega}_R^{R_0} = \vec{\Omega}_{R_s}^{R_0} + \vec{\Omega}_R^{R_s} = \begin{Bmatrix} \dot{\alpha}_s \\ \dot{\beta}_s \\ \dot{\gamma}_s \end{Bmatrix}_{R_s} + \begin{Bmatrix} 0 \\ 0 \\ \dot{\psi} \end{Bmatrix}_{R_s} + \begin{Bmatrix} \dot{\theta} \\ 0 \\ 0 \end{Bmatrix}_{R_2} + \begin{Bmatrix} 0 \\ \dot{\phi} \\ 0 \end{Bmatrix}_R = \begin{Bmatrix} \omega_x \\ \omega_y \\ \omega_z \end{Bmatrix}_R \tag{6}$$

$$I_D = \begin{bmatrix} I_{Dx} & 0 & 0 \\ 0 & I_{Dy} & 0 \\ 0 & 0 & I_{Dz} \end{bmatrix} \tag{7}$$

being I_{Dx}, I_{Dy}, and I_{Dz}, are the mass inertia moments of the disc. ω_x, ω_y, and ω_z, are the angular velocities of the frame R with respect to the frame R_0 (Duchemin, 2003).

The kinetic energy expressions for the shaft and unbalanced mass m_u are given by:

$$\begin{gathered} T_S = \frac{1}{2}\rho S \int_0^L \left(\dot{u}_s^2 + \dot{v}_s^2 + \dot{w}_s^2\right) dy + \frac{1}{2}\rho \int_0^L \left[I_x\,\omega_x^2 + I_y \omega_y^2 + I_z\,\omega_z^2\right] dy \\ T_u = \frac{1}{2} m_u \left(\vec{V}_{DR_s}^{R_0}\right)^2 \end{gathered} \tag{8}$$

where T_S and T_u are the kinetic energies of the shaft and unbalanced mass, respectively. The translations u_s, v_s, and w_s, are similar to the ones presented by Eq. (5) (i.e., time derivatives of u_C, v_C, and w_C, respectively), regarding any y position along the shaft (see Fig. 1). I_x, I_y, and I_z, are the area inertia moments of the shaft. The parameter ρ is the volumetric density of the shaft material, E is the Young's Modulus, and S stands to the cross-section area of the shaft. Additionally,

$$\vec{V}_{DR_s}^{R_0} = \left(\frac{d\overrightarrow{OD}}{dt}\right)_{R_s} + \vec{\Omega}_{R_s}^{R_0} \times \left(\overrightarrow{OD}\right)_{R_s} = \begin{Bmatrix} \dot{X} + \dot{u} + d\Omega\cos\Omega t + \dot{\beta}_s\left(Z + w + d\Omega\cos\Omega t\right) - \dot{\gamma}_s\left(Y + y\right) \\ \dot{Y} + \dot{\gamma}_s\left(X + u + d\Omega\sin\Omega t\right) - \dot{\alpha}_s\left(Z + w + d\Omega\cos\Omega t\right) \\ \dot{Z} + \dot{w} - d\Omega\sin\Omega t + \dot{\alpha}_s\left(Y + y\right) - \dot{\beta}_s\left(X + u - d\Omega\sin\Omega t\right) \end{Bmatrix}_{R_s} \tag{9}$$

where $\vec{V}_{DR_s}^{R_0}$ is the translational velocity of the point D with respect to R_0 expressed in R_s (see Fig. 3). Ω is the rotation speed of the rotor, t is the time vector, and d is the distance of m_u from the geometric center of the shaft.

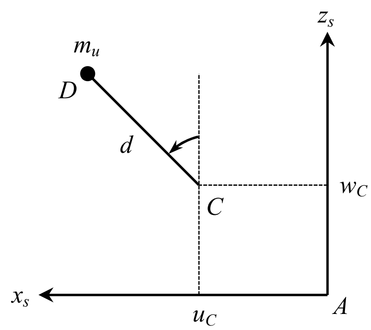

Figure 3. Unbalanced mass.

It is worth mentioning that the strain energy U of the shaft is not modified by the movement of the rotor base (i.e., translations and rotations), since it do not depend of the constraints associated with the onboard rotor problem. Thus,

$$U = \frac{1}{2}EI_m\int_0^L\left[\left(\frac{\partial^2 u}{\partial y^2}\right)^2 + \left(\frac{\partial^2 w}{\partial y^2}\right)^2\right]dy + \frac{1}{2}EI_a\int_0^L\left\{\left[\left(\frac{\partial^2 w}{\partial y^2}\right)^2 - \left(\frac{\partial^2 u}{\partial y^2}\right)^2\right]\cos 2\Omega t + 2\frac{\partial^2 u}{\partial y^2}\frac{\partial^2 w}{\partial y^2}\cos 2\Omega t\right\}dy$$

$$I_m = \frac{I_x + I_z}{2} \qquad I_a = \frac{I_x - I_z}{2} \tag{10}$$

where E is the Young's Modulus associated with the shaft material.

As mentioned, the mathematical model of the rotor used in this work is derived from the Lagrange's equations and the Rayleigh-Ritz method. The rotor is assumed to be simply supported at both ends. Therefore, the displacements along the x_s and z_s directions, considering any y location along the shaft (see Fig. 1), are given by:

$$u(y,t) = f_1(y)q_{11}(t) + f_2(y)q_{12}(t)$$
$$w(y,t) = f_1(y)q_{21}(t) + f_2(y)q_{22}(t) \tag{11}$$

in which q is a generalized independent coordinate (Lalanne and Ferraris, 1998).

In this work, two displacement functions $f(y)$ are considered to determine the vibration responses of the rotor. The first and second vibration modes of a simple supported beam in bending are represented (beam with constant cross section). Thus, q_{11} and q_{21} from Eq. (11) are associated with the displacement function $f_1(y)$. The coordinates q_{12} and q_{22} are related with $f_2(y)$. The displacement functions can be seen in Eq. (12)

$$f_1(y) = \sin\frac{\pi y}{L}$$
$$f_2(y) = \sin\frac{2\pi y}{L} \tag{12}$$

The angular rotations θ and ψ are small and they can be approximated by

$$\theta(y,t) = \frac{d\,f_1(y)}{dy} q_{21}(t) + \frac{d\,f_2(y)}{dy} q_{22}(t)$$

$$\psi(y,t) = -\frac{d\,f_1(y)}{dy} q_{11}(t) - \frac{d\,f_2(y)}{dy} q_{12}(t) \tag{13}$$

Introducing the Eq. (11) and Eq. (13) into the kinetic and strain energies of the rotor (i.e., determination of the vibration responses from $f_1(y)$ and $f_2(y)$ separately), the Lagrange's equations are applied leading to

$$M_{f_1(y)} \begin{Bmatrix} \ddot{q}_{11} \\ \ddot{q}_{21} \end{Bmatrix} + C_{f_1(y)} \begin{Bmatrix} \dot{q}_{11} \\ \dot{q}_{21} \end{Bmatrix} + K_{f_1(y)} \begin{Bmatrix} q_{11} \\ q_{21} \end{Bmatrix} = \begin{Bmatrix} F_1 \\ F_2 \end{Bmatrix}_{f_1(y)} = F_{f_1(y)} \tag{14}$$

$$M_{f_2(y)} \begin{Bmatrix} \ddot{q}_{12} \\ \ddot{q}_{22} \end{Bmatrix} + C_{f_2(y)} \begin{Bmatrix} \dot{q}_{12} \\ \dot{q}_{22} \end{Bmatrix} + K_{f_2(y)} \begin{Bmatrix} q_{12} \\ q_{22} \end{Bmatrix} = \begin{Bmatrix} F_1 \\ F_2 \end{Bmatrix}_{f_2(y)} = F_{f_2(y)} \tag{15}$$

where M, C, and K, are the mass, stiffness, and gyroscopic/damping matrices, respectively (matrices related to each displacement function). The vector F contains the unbalance force and some additional terms due to the movement of the rotor base. Similarly, additional terms are incorporated to the matrices K and C (Duchemin, 2003). The gravitational load was disregarded in this contribution.

3. NUMERICAL RESULTS

As shown above, figure 1 presents the rotating machine used in the numerical simulations studied in this work. It is composed of a flexible steel shaft with 400 mm length and 20 mm diameter (E = 200 GPa, ρ = 7800 kg/m^3) and one rigid disc of steel and with 300 mm of diameter and 30 mm of thickness (ρ = 7800 kg/m^3) positioned at y = 133.33 mm. The rotor is simply supported at points A and B (representation of the bearings). The rotating parts take into account a proportional damping to the stiffness matrix incorporated in Eq. (15) ($C_p = \beta_p K$), considering $\beta_p = 2 \times 10^{-4}$. An unbalance of 1500 g.mm at 0^o applied to the disc of the rotor was considered. Figure 4 shows the Campbell diagram of the considered rotor, in which the three first critical speeds in the analyzed frequency band are, approximately, 2510 rev/min, 3090 rev/min, and 7600 rev/min (i.e., backward and forward whirls disregarding the base excitations).

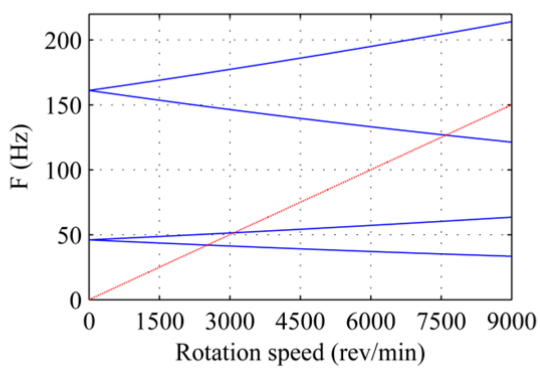

Figure 4. Campbell diagram of the analyzed rotor.

Figure 5 shows the vibration responses of the rotor measured along the x_s and z_s directions at the disc position (i.e., u_C and w_C) considering the system under four different conditions: base at rest, constant acceleration of 0.5 m/s^2, 1.0 m/s^2, and 2.0 m/s^2 (Fig. 5a, Fig. 5b, Fig. 5c, and Fig. 5d, respectively). The accelerations were imposed along the z_0 direction (see Fig. 1). In all scenarios, the determined vibration responses of the rotor operating at 1200 rev/min were analyzed. As expected, only the w_C vibration responses change according to the increasing acceleration. Additionally, it is worth mentioning that the peak-to-peak vibration amplitudes associated with the w_C direction changes when the acceleration of the base is taken into account, as showed by Tab. 1.

Table 1. Peak-to-peak vibration amplitudes determined for u_C and w_C directions.

Acceleration $\ddot{Z}$	u_C (m)	w_C (m)
0		2.39×10^{-7}
0.5	2.39×10^{-7}	4.02×10^{-7}
1.0		4.02×10^{-7}
2.0		4.02×10^{-7}

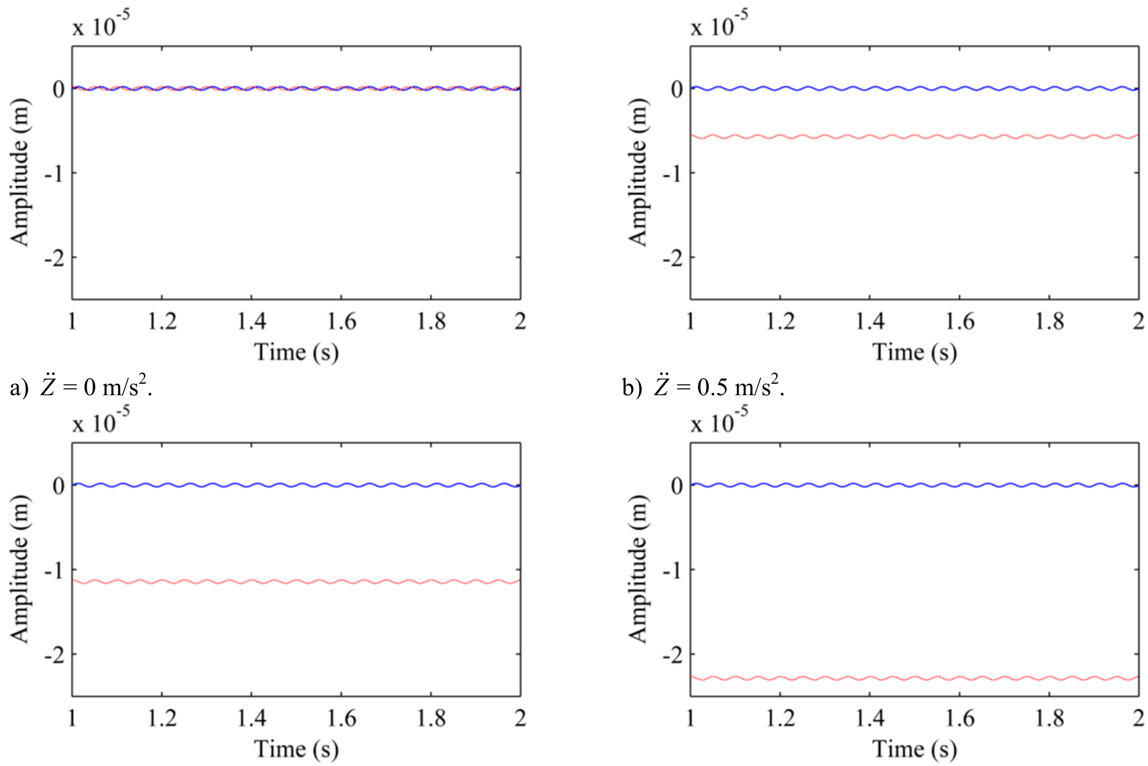

a) $\ddot{Z}$ = 0 m/s^2. b) $\ddot{Z}$ = 0.5 m/s^2. c) $\ddot{Z}$ = 1.0 m/s^2. d) $\ddot{Z}$ = 2.0 m/s^2.

Figure 5. Vibration responses of the rotor considering a base acceleration (—— u_C; -------- w_C).

Figure 6 shows the vibration responses of the rotor measured along the x_s and z_s directions at the disc position considering the system under two different conditions, regarding the displacement of the base along the x_0 and z_0 directions (see Fig. 6b and Fig. 6d, respectively). The associated vibration responses are shown by Fig. 6a and Fig.6b, respectively. In all scenarios, the determined vibration responses of the rotor operating at 1200 rev/min were analyzed. Note that both u_C and w_C responses are changed with the imposed displacements on the base. Clearly, u_C is more affected than w_C when the displacement of the base along the x_0 is considered (and vice-versa).

Figure 7 shows the orbits determined for the disc considering a sinusoidal excitation imposed along the direction x_s, as given by:

$$\alpha_s = \Lambda \sin\left(2\pi n \Omega t\right) \tag{16}$$

where Λ is equal to 5 degrees (i.e., angular rotation) and n is a constant used to produce an asynchronous base excitation. Considering the rotor operating at 1200 rev/min, Fig. 7a, Fig. 7b, and Fig. 7c, show the orbits obtained by using n = 2, n = 3, and n = 4, respectively. Note that internal loops occurs when the base rotation are considered. Figure 8 shows the orbits determined in the disc of the rotor considering the same excitation conditions used to determine the orbits presented in Fig. 7, however, for the rotor operating at 1545 rev/min (i.e., half of the first forward critical speed). The internal loops can also be observed with the rotor operating under these consditions. In all scenarios, the scale of the horizontal and vertical axis are different in order to provided a better visualization of the orbits.

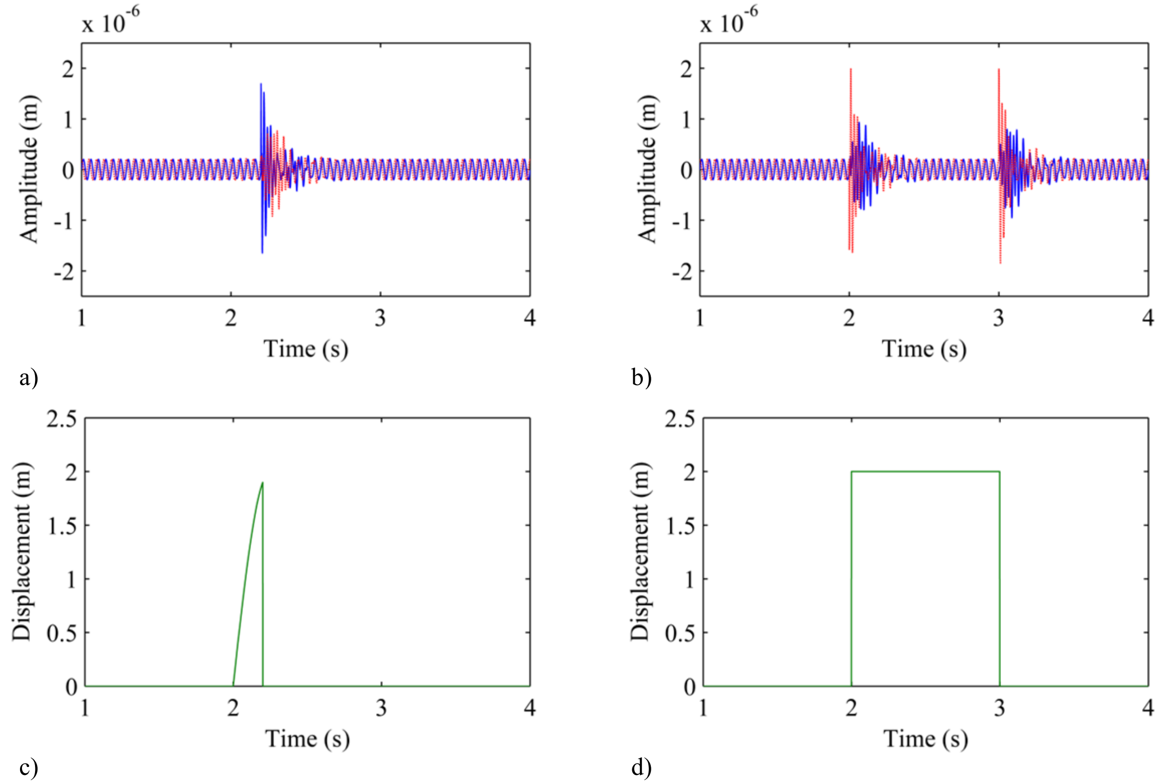

Figure 6. Vibration responses of the rotor considering a base displacement (—— u_C; ------ w_C; —— displacement).

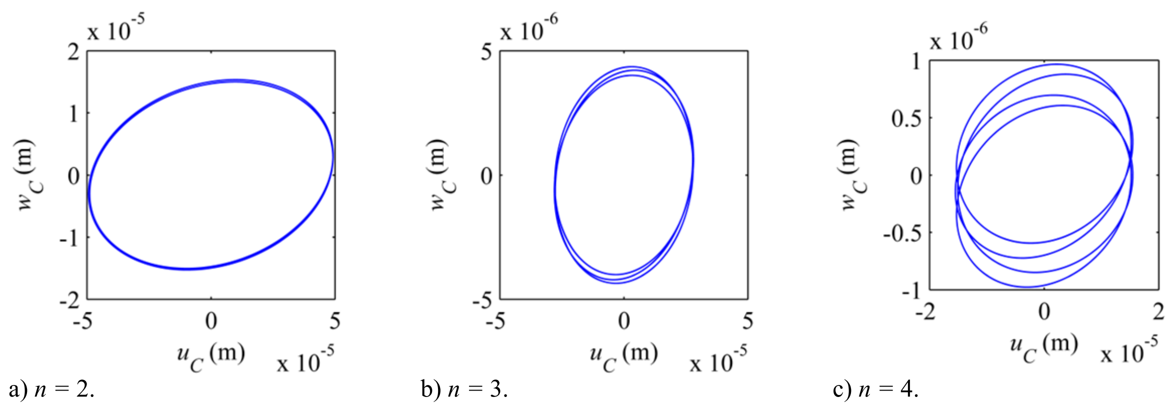

Figure 7. Orbits determined for the disc for the rotor operating at 1200 rev/min under a base sinusoidal excitation.

4. CONCLUSION

In this paper, a preliminary investigation regarding the dynamic behavior of a rotor system subjected to a base excitation was discussed. The rotating machine used in the numerical analyzes is composed by a horizontal flexible shaft, one rigid disc, and two self-aligning ball bearings. The mathematical model of the rotor was derived from the Lagrange's equations and the Rayleigh-Ritz method. The proposed analyses were performed both in the time and frequency domains, as represented by the orbits, unbalance response, and the Campbell diagram. The orbits and unbalance responses were determined from different base excitations, so that the discrepancies between regular rotor and onboard rotor were analyzed. Regarding the Campbell diagram, it was obtained disregarding the base excitation. Further studies will encompass evaluations based on a finite element model for the rotor. An experimental verification is also scheduled.

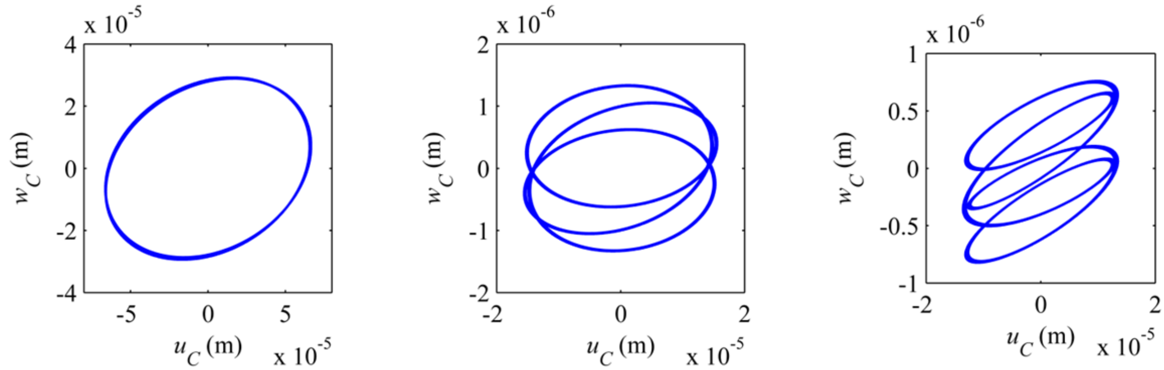

a) n = 2. b) n = 3. c) n = 4.

Figure 8. Orbits determined in the disc for the rotor operating at 1545 rev/min under a base sinusoidal excitation.

5. ACKNOWLEDGEMENTS

The authors are thankful to the Brazilian Research Agencies FAPEMIG and CNPq (INCT-EIE) and also to CAPES for the financial support provided to this research effort.

6. REFERENCES

Dakel, M., Baguet, S., Dufour, R., 2014, "Bifurcation analysis of a non-linear on-board rotor-bearing system". In: P*roceeding of the International Design Engineering Technical Conferences & Computers and Information in Engineering Conference*, *IDETC/CIE*. Buffalo, New York, USA.
Dunchemim, M., Berlioz, A., Ferraris, G., 2006. "Dynamic behavior and stability of a rotor under base excitation". *ASME,* Vol. 128, p. 576.
Dunchemim, M., 2003, *Contribuition à l'étude du comportement dynamic d'un rotor embarqué.* Ph.D. thesis, INSA Lyon, Lyon.
Dunkerley, S., 1984, 1984, "On the whirling and vibration of shaft". *Philosophical Transactions of the Royal Society of London*, Vol. 195, n. 1, p. 279-359.
El-Saeidy, F.M.A., Sticher, F., 2010, "Dynamics of a rigid rotor linear/nonlinear bearings system subject to rotating unbalance and base excitations". *Journal of Vibration and Control*, Vol. 16, n. 3, p. 403-438.
Hankine, B.J.M., 1869, "On the centrifugal force of rotating shafts". *The Engineer*, Vol. 1, n. 1, p. 1.
Ishida, Y., Yamamoto, T., 2012. *Linear and nonlinear rotordynamics*. Wiley-VCH.
Jeffcott, H.H., 1919, "The lateral vibration of loaded shafts in the neighborhood of a whirling speed: the effect of want of balance". *Philosophical Magazine A*, Vol. 37, n. 1, p. 304-315.
Lalanne, M., Ferraris, G., 1998. *Rotordynamics prediction in engineering*. John Wiley & Sons, INC.
Lallement, G., Lecoanet, H., Steffen Jr, V., 1982, "Vibrations de rotors sur paliers à matrice de raideur non symetrique". *Machine and Mechanism Theory*, Vol. 17, n. 1, p. 47-55.
Nelson, H.D., Macvaugh, J.M., 1976, "The dynamics of rotor bearing systems using finite elements". *Journal of Engineering for Industry*, Vol. 98, n. 2, p. 593-600.

7. RESPONSIBILITY NOTICE

The authors are the only responsible for the printed material included in this paper.